1 *Article*

2 Aerosol from Biomass Combustion in Northern
3 Europe: Influence of Meteorological Conditions and
4 Air Mass History

5 **Jun Noda[1,a], Robert Bergström[1,2,3], Xiangrui Kong[1], Torbjörn L. Gustafsson[1], Borka Kovacevik[1,b],**
6 **Maria Svane[1,c], and Jan B. C. Pettersson[1,4]***

7 [1] Department of Chemistry and Molecular Biology, Atmospheric Science, University of Gothenburg, SE - 412
8 96 Gothenburg, Sweden
9 [2] Swedish Meteorological and Hydrological Institute, SE - 601 76 Norrköping, Sweden
10 [3] Department of Space, Earth and Environment, Chalmers University of Technology, SE-412 96 Gothenburg,
11 Sweden
12 [4] Gothenburg Centre for Sustainable Development, GMV Chalmers University of Technology & University
13 of Gothenburg, Aschebergsgatan 44, SE- 412 96 Göteborg, Sweden
14
15 [a] School of Veterinary Medicine, Rakuno Gakuen University, Ebetsu, Hokkaido 069-8501, Japan
16 [b] Belnigo Konsulting, str.Boris Sarafov 42/2/8, Skopje, RN Macedonia
17 [c] Gothenburg Centre for Sustainable Development, GMV Chalmers University of Technology & University
18 of Gothenburg, Aschebergsgatan 44, SE- 412 96 Göteborg, Sweden
19
20 ***** *Correspondence: Jan Pettersson (janp@chem.gu.se)*

21 **Abstract:** Alkali-containing submicron particles were measured continuously during three months,
22 including late winter and spring seasons in Gothenburg, Sweden. The overall aims were to
23 characterize the ambient concentrations of combustion-related aerosol particles and to address the
24 importance of local emissions and long-range transport for the atmospheric concentrations in the
25 urban background environment. K and Na concentrations in the PM_1 size range were measured by
26 an alkali aerosol mass spectrometer (Alkali-AMS) and a cluster analysis was conducted. Local
27 meteorological conditions and some other data sets were obtained, and back trajectory analyses
28 and chemical transport model (CTM) simulations were included for the evaluation. The
29 Alkali-AMS cluster analysis indicated three major clusters: 1) biomass burning origin, 2) mixture of
30 other combustion sources, and 3) marine origin. Low temperatures and low wind speed conditions
31 correlated with high concentrations of K-containing particles, mainly due to regional emissions
32 from residential biomass combustion; transport of air masses from continental Europe also
33 contribute to cluster 1. The CTM results indicate that open biomass burning in the eastern parts of
34 Europe may have contributed substantially to high $PM_{2.5}$ concentrations (and to cluster 1) during
35 an episode in late March. According to the CTM results the mixed cluster (2) is likely to include
36 particles emitted from different source types and no single geographical source region seems to
37 dominate for this cluster. The back trajectory analysis and meteorological conditions indicated that
38 the marine origin cluster was correlated with westerly winds and high wind speed; this cluster had
39 high concentrations of Na-containing particles, as expected for sea salt particles.

40 **Keywords:** biomass burning; residential wood combustion; aerosol mass spectrometry; potassium;
41 chemical transport model
42

43 1. Introduction

44 Burning of wood and other biomass fuels for heating and cooking purposes is common around
45 the globe [1]. Although biomass burning in fireplaces and wood stoves are such common processes,
46 the knowledge about the influences on health is still fairly limited. Many epidemiological studies

have demonstrated that ambient particulate matter (PM) may cause health problems [2,3]. Biomass burning and wood smoke from the combustion may pose considerable risk to respiratory and other aspects of human health, e.g., pneumotoxicity and other health problems [4,5]. It is important to characterize the PM exposure from biomass burning and other sources, to understand the health risk of PM. Viana *et al*. [6] reviewed studies dealing with source apportionment of atmospheric particulate matter in Europe between 1987 and 2007. They showed that studies throughout Europe agreed on the identification of four main source types: 1) a vehicular source, 2) a crustal source, 3) sea spray, and 4) a mixed industrial/fuel-oil combustion and secondary inorganic aerosol. Other sources, such as biomass combustion, were rarely identified with the methods traditionally employed, even though they may contribute significantly to PM levels in specific locations [7-12].

The most commonly used tracers for biomass burning are levoglucosan (LG) [13-19] and potassium [15,16,18]. LG is the product from pyrolysis of cellulose, and potassium, as one of the main nutrient elements, is released from the biomass during burning. A difference between the two tracers is that LG is only emitted during the ignition stage, as LG breaks down into smaller molecules at high temperatures [20,21] while the emission of alkali remain during the whole burning process. Aerosol mass spectrometers (AMS) provide the aerosol composition in ambient air and allow for studies on time-scales that are relevant for aerosol processes in the atmosphere [22-26]. We have developed an Alkali AMS technique based on surface ionization (SI) of particle-bound components [27,28]. Briefly, with this method, aerosol particles are vaporized on a hot metal surface, and the SI technique efficiently ionizes elements with low ionization potentials. Highly sensitive and selective detection can be achieved, and characterization of the alkali metal content in individual particles with diameters down to 14 nm has been demonstrated [27]. The Alkali AMS has previously been applied in field studies in urban air [29] and studies of large-scale biomass combustion [30,31]. The single-particle characterization significantly improves the chances of on-line identification of combustion aerosol and sea spray particles in ambient air. Long-time series of aerosol measurements from residential wood combustion and other solid fuel combustion sources are rare. In comparison to the use of other tracer substances, the alkali detection has the advantage that the compounds remain stable in the atmospheric environment — oxidation and UV irradiation will not change them. In contrast, the common marker compound, levoglucosan has the disadvantage that one needs to consider its reactions in the atmosphere [32,33].

This work describes the results from continuous AMS measurements of alkali-containing submicron particles in Gothenburg, Sweden, during three months period from February 16 to May 20, 2007. The overall aims are to characterize the ambient concentrations of combustion-related aerosol particles during a relatively long period, including the winter and spring seasons, and to address the importance of local emissions and long-range transport for the atmospheric concentrations in the urban background environment. The AMS results are compared to meteorological data, cluster analysis of back trajectories, and results from the EMEP MSC-W chemical transport model [34] to relate the observations to air mass origin and emission source categories.

2. Methods

2.1 Measurement site

The studies were performed in the city of Gothenburg, which is located on the west coast of Sweden and has a population of about 600,000 people. The AMS measurements were conducted at the atmospheric science center laboratory at the university campus (57.6911°N 11.9780°E). The campus is in close proximity to the downtown area and may be characterized as an urban background site. The laboratory is situated on the 4th floor and has access to a roof immediately outside the laboratory windows. It is facing a relatively wide street canyon with a two-lane paved local road. The sampled aerosol (1.0 L min^{-1}) was directed to the inlet of the AMS instrument through a 1 m long copper tube (i.d. 0.9 cm) on the outside of the wall and connected to 0.75 m of conducting tubing (i.d. 0.6 cm) inside the laboratory.

2.2 Alkali aerosol mass spectrometer measurements

The Alkali AMS used for on-line measurements of alkali-containing particles has been described in detail elsewhere [27,28]. Briefly, aerosol particles are drawn into the vacuum system of the AMS through a standard aerodynamic lens system [35,36], which produces a sharply focused particle beam with high transmission of particles into the detection unit [27,37]. The upper particle diameter limit is about 1 μm and the transmitted aerosol mass corresponds approximately to PM1 (total mass concentration of particles with a diameter < 1 μm) in the same way as for other widely used AMS systems [37,38]. The lower particle size limit is below 20 nm, which is lower than for the Aerodyne AMS because of a shorter distance (70 mm) from the outlet of the lens system to the ionizing unit in the present instrument.

The particle beam is directed onto a hot platinum (Pt) vaporizer in the detection chamber of the Alkali AMS [28]. The Pt vaporizer is designed as a small open box (3×3×5 mm), and the construction avoids problems caused by particle bouncing effects [27]. Individual particles decompose in contact with the hot surface, and the alkali metal content of the particles desorbs in ionic form from the metal surface, a phenomenon known as the surface ionization (SI) described in Ionov [39] and Zandberg [40]. The ionization probability is determined by the difference between the work function of the metal and the ionization potential of the desorbing compound. The alkali metals have unusually low ionization potentials, and the ionization probability approaches 100%, while desorption in neutral form dominates completely for other type of elements. During the experiments, the Pt surface was heated to a temperature of 1500 K, and the decomposition of an individual alkali salt particle on the hot surface typically resulted in the emission of alkali ions during 0.1–1 ms [27]. Particles consisting of alkali compounds that rapidly decompose and desorb at 1500 K are efficiently detected, including sea spray particles and typical aerosol particles produced by biomass and coal combustion. Combustion of biomass and coal results in a significant release of alkali-containing compounds, which subsequently re-condense into particles as the flue gases are cooled [27, 28, 31]. In contrast, strongly bound compounds including alkali silicates and aluminates that may be found in mineral dust and ash particles would require a considerably higher Pt vaporizer temperature to be efficiently detected by the Alkali AMS.

An orthogonal acceleration time-of-flight mass spectrometer (oa-TOFMS) was used to measure alkali ion mass spectra for individual nanometer-size aerosol particles [28]. One thousand consecutive 13.5 μs mass spectra scans were added and stored every 13.5 ms by a computer-controlled multi-channel scaler (FAST ComTec P7882, 200 MHz discriminator). A total of approximately $6 \cdot 10^8$ mass spectra were generated during the field campaign. The majority of the mass spectra only contained a low background signal, while occasionally a millisecond burst of ions was detected from a decomposing particle. The count rate of alkali-containing particles was typically low enough to make particle coincidence negligible, and the data set thus contains information about the Na and K content of single particles. The AMS was calibrated, and its operation was regularly controlled using laboratory-generated particles with known alkali salt content following the procedure described by Svane *et al*. [28].

2.3 Supporting measurements

The Environmental Office in Gothenburg provided trace gas, PM2.5, PM10, and meteorological data with a temporal resolution of 6 min. The measurements were performed 2 km from the campus at the urban background station "Femman" in the city center (57.7085° N; 11.9701° E), which is situated on a building with a flat roof and a height of 25 m. Additional meteorological measurements (Vaisala Inc., Model WXT510) performed at the AMS measurement site agreed well with the data from the Environmental Office.

2.4 Cluster analysis of mass spectra

The Na and K peaks in individual mass spectra were integrated, and mass spectra with zero signals for both ions were discarded. This reduced the data set to $9 \cdot 10^7$ mass spectra corresponding

146   to individual aerosol particles with a detectable Na and/or K content. The large size of the data set
147   makes traditional clustering analysis techniques inapplicable, or at least highly impractical, and it
148   was necessary to apply an alternative method. Three data clusters were initially qualitatively
149   identified based on a density-based map of the complete data set indicated in Figure 1. In the next
150   step, the density-based clustering approach DBSCAN (Density-Based Clustering of Applications
151   with Noise) approach was used to extract the desired clusters and normalize them into templates
152   [41,42]. The density-based clustering approach utilizes a local cluster criterion, and clusters are
153   defined as regions in data space where the objects are dense and remain separated from one another
154   by low-density regions [42]. DBSCAN can describe arbitrarily shaped clusters, and the method has
155   been applied to AMS data and compared with the ART-2a method [41,60]. Finally, the boundaries of
156   the three clusters were described by non-linear functions, as illustrated in Figure 1. A fraction with
157   both low Na and K content was also discarded to avoid potential influence of noise in the data
158   (Figure S1). A more detailed analysis of daily data sets shows that Cluster 1 and 3 are consistently
159   described by the clusters indicated in Figure 1. On the other hand, Cluster 2 with both high K and Na
160   content includes several overlapping sub-clusters (examples can be found in Figure S2), which
161   suggests that this factor include contributions from a group of sources. As described below, Clusters
162   1 can be associated with residential wood combustion, Cluster 2 with a mixture of other combustion
163   sources, and Cluster 3 with sea spray.

164   *2.5 Air mass back-trajectories*

165   Backward 72h trajectories ending 500 m above ground level in Gothenburg were calculated
166   using the HYSPLIT4 model [43]. New trajectories were started every 6 h, giving a total of 376
167   trajectories for the entire measurement period. The trajectories were analyzed by cluster analysis
168   using the built-in analysis module of the HYSPLIT program. The clustering process is an iterative
169   process wherein each step, the two closest clusters (trajectories) are paired until all trajectories are
170   collected in one cluster [43]. The change in total spatial variance is calculated for each clustering step,
171   and a large change in spatial variance indicates that two relatively different clusters (trajectories)
172   have been paired. Large changes in variance occurred in the formation of 5 and 10 clusters, which
173   suggested that solutions with 6 and 11 clusters provided useful solutions in the clustering analysis.
174   Results from the smaller six-cluster solution are used in the present study.

175   *2.6 Chemical transport modelling*

176   The EMEP MSC-W chemical transport model (CTM) [44,34,45] was used to track influences of
177   different emission sources that may contribute to the observed K and Na concentrations in
178   Gothenburg. The model is used in many different applications and includes treatment of the most
179   important gases for describing photochemical ozone formation and secondary production of aerosol
180   particles from anthropogenic and biogenic sources [46-50]. Primary emissions of particles from
181   anthropogenic sources, sea salt, and wind-blown dust are also included in the model. Emissions of
182   alkali compounds are not explicitly included in the model (except Na from sea salt). In the present
183   work, regional-scale simulations were performed with the EMEP MSC-W CTM using a model
184   domain that covers all of Europe and large parts of the North Atlantic Ocean and the Arctic area.
185   The EMEP model results used in this study are mostly taken from the model simulations
186   described by Bergström *et al*. [51]. The EMEP MSC-W model was run with a relatively coarse
187   resolution; each grid point covered an area of about 50 km × 50 km, and the lowest model layer was
188   ca. 90 m thick. This limits the ability to model the impact of local emission sources in detail since the
189   emissions will be diluted over an area of ca 2500 km^2. The model will thus underestimate impacts
190   from point (and small area) sources near the measurement site. The anthropogenic model emissions
191   were handled as in Genberg *et al*. [48]; primary carbonaceous aerosol emissions from residential
192   combustion were taken from the new emission inventory by TNO [8]; other primary carbonaceous
193   aerosol emissions are taken from the EUCAARI inventory [8]; other anthropogenic emissions were
194   taken from the standard EMEP emission inventory [34, 52]. Emissions from open biomass fires (both
195   wildfires and agricultural burning) were taken from the Fire Inventory from NCAR version 1.0

196   (FINNv1) [53]. Natural emissions of biogenic volatile organic compounds from vegetation and sea
197   salt from the oceans are calculated within the model [34].
198   The temporal distribution of the emissions is described in detail by Simpson *et al.* [34]; for small
199   scale non-industrial combustion (SNAP-sector 2; dominated by residential combustion) the
200   day-to-day variation of the emissions are based on the heating degree day concept, which means
201   that the emissions depend on the daily temperatures in the respective emission areas [34].

3. Results and Discussion

3.1 Overview of measured K and Na concentrations

204   Figure 2 shows an overview of the Na and K concentrations measured during the period from
205   February 16 to May 20, 2007, together with meteorological, PM10, and NOx data. The Na and K
206   concentrations are typically in the range 1–50 ng m^{-3} and show large variability on the time scale of a
207   few hours for both elements with peak concentrations above 100 ng m^{-3} for Na. The time series
208   indicate that the two concentrations are correlated during some periods, but this is not generally true
209   and the Na:K ratio usually varies in the range from 0.1 to 20. The alkali concentrations do not appear
210   to show a general trend related to seasonal changes, and the reasons for the observed concentration
211   variability are instead to be sought in the changes in atmospheric conditions and source strengths.

3.2 Influence of local meteorological conditions

213   The meteorological conditions changed from winter to spring during the measurement period,
214   and the monthly average temperatures were 0.5, 6.0, 9.1, and 12.0 °C during February, March, April,
215   and May, respectively. The temperatures were close to the normal monthly averages for February
216   and May while March was 4 °C and April was 2 °C warmer than normal. Daily temperatures were
217   below zero during several days in February, and peak day-time temperatures were in the range of 15
218   to 20 °C during some of the warmer periods. Ground-level temperature inversions are well known
219   to have a strong influence on air quality in Gothenburg [54,55] and several strong inversions and
220   associated periods of poor air quality occurred in March, while the effects of inversions on air
221   quality were less important during other periods.
222   Figure 3 shows that the local wind speed has a relatively strong effect on the mean Na and K
223   concentrations. Na concentrations increase considerably with wind speed above 3 m s^{-1}, while the
224   highest K concentrations are observed with wind speeds below 3 m s^{-1}. Figure 4 illustrates that the
225   wind direction also has an important effect on the concentrations of alkali-containing particles. High
226   concentrations of Na-containing particles are observed with westerly winds from the nearby sea,
227   while the highest K concentrations are observed for easterly winds from the inland region. Figure 5
228   shows that local temperature also has a substantial impact on the K concentrations. The
229   concentrations of K (and Na) increase with decreasing temperature below 2 °C. The observed
230   correlations between high Na concentrations and high wind speeds and westerly winds strongly
231   indicate that the observed Na-rich particles mainly consist of sea salt particles. High K
232   concentrations are, on the other hand, favored by low temperatures, low wind speeds and winds
233   from the inland, which suggests that they may originate from biomass burning in the nearby region
234   during cold periods. It appears that the local meteorological conditions have an important impact on
235   the concentrations of Na and K in PM1. However, the observed concentrations show large variations
236   under similar meteorological conditions, which indicates that regional production of particles may
237   not be sufficient to explain the observations.

3.3 Influence of air mass history

239   To further evaluate the origin of the detected particles, back trajectories of air masses reaching
240   Gothenburg were calculated and analyzed by group analysis. The results from a six-group solution
241   are presented in Figure 6, where the traces for individual back trajectories are indicated. Figure 7
242   shows the resulting mean trajectories for the six group solutions and the relative contribution to each
243   cluster in percent. Some of the clusters consist of trajectories with a complex pattern while some

244   were more directed from a certain region. The individual clusters are attributed to different regions
245   of origin for the air masses: Central (C), Eastern (E), Northern (N), and Western Europe (W), as well
246   as clusters with Atlantic (A) and Polar (P) origin.

247   Table 1 summarizes mean values for the alkali, PM10, and trace gas concentrations depending
248   on the type of air mass reaching Gothenburg together with mean meteorological data. These data
249   sets are only included from time periods where at least two consecutive air mass trajectories are
250   attributed to the same group type. The highest mean Na concentration and the highest Na:K ratio
251   are observed in air masses with an Atlantic origin (trajectory cluster No. 5). The highest mean K
252   concentrations and lowest Na:K ratios are observed when the air masses have an Eastern or Central
253   European origin. In these cases, the observed Na:K ratios are consistent with alkali-containing
254   particles originating from solid fuel combustion processes [30,31]. NO, NOx and PM10
255   concentrations are also high for air mass types 1 and 2 compared to other types of air masses. The air
256   masses originating from Northern and Western Europe, as well as from the Polar region appear to
257   consist of local polluted air with different degrees of marine character.

258   To further address the importance of regional emissions and long-range transport, results from
259   a short episode (March 24 to April 2, 2007) are illustrated in Figure 8 and 9. The period is
260   characterized by large daily variations in temperature and relatively strong night-time temperature
261   inversions. Figure 8a shows that the air masses reaching Gothenburg during this period originated
262   in Eastern Europe, while the air mass origin shifted before and after this period. In addition to solid
263   fuel combustion, fires are common in Eastern Europe during this period of the year due to
264   agricultural burns and may potentially influence air quality in Northern Europe during short
265   episodes. Figure 8b shows the distribution of fires in Europe (at 1 km resolution) during the short
266   episode, where each dot on the map indicates a fire detected with the moderate resolution imaging
267   spectroradiometer (MODIS) aboard the Terra satellite [56].

268   Figure 9a shows a close up of the measured Na and K concentrations together with wind
269   direction (Figure 9b) and wind speed (Figure 9c) data during the same period as covered in Figure 8.
270   The K concentration was relatively high during this period, while Na was low during most of the
271   period. An interesting effect was that both K and Na appear to follow a diurnal pattern during this
272   particular period, an effect that was not observed during other parts of the measurement campaign.
273   For the K concentrations, often reached its highest values before noon, while Na peaked during the
274   evening. The wind direction data (Figure 9b) indicates that the increase in Na concentration was
275   related to a weak sea breeze that was observed daily in the afternoon and evening. The wind speed
276   increased slightly during the sea breeze, but it was fairly low, and the Na signal may be attributed
277   with limited formation of sea salt particles in the region near Gothenburg. The modulated K signal
278   was likely due to a combination of long-range transport and regional emissions from biomass
279   burning that were trapped near the ground during the relatively cold nights with strong night-time
280   temperature inversions.

281   The results in Figure 10 indicate that the concentrations of Na and K are in general correlated in
282   spite of occasional variations. Cluster 1 has a closer linkage in the winter season while Cluster 2 has
283   no apparent seasonal trend coupling. This agrees with the temperature dependence of K mass
284   concentrations illustrated in Figure 11a, which shows that low temperatures favor Cluster 1, while
285   Cluster 2 shows no clear dependence on temperature. They are both favored by low wind speeds
286   (Figure 11b).

287   *3.4 Comparison between Alkali AMS and chemical transport modeling results*

288   The experimental data are compared with results from model simulations with the EMEP
289   MSC-W CTM, with special emphasis on the influence of biomass burning and fossil fuel combustion.
290   Figure 12 shows the measured total concentration of PM2.5 at the urban background station
291   Femman and the modeled total concentration of carbonaceous PM from biomass burning (the sum
292   of organic aerosol and elemental carbon from residential biomass combustion and open biomass
293   fires). During the period 17 February – 20 May 2007, the measured hourly PM2.5 concentration
294   varies from 0 to about 50 $\mu g\ m^{-3}$, and the highest concentrations occur during a handful of major

295 peaks. The highest PM2.5 concentrations were observed during the period 23 March – 2 April (two
296 concentration peaks) — at the same time the modeled concentration of particles from open fire and
297 residential biomass burning is also high. There is a relatively high degree of correlation between the
298 measured PM2.5 and the modeled biomass burning PM during the campaign period (r = 0.81, for
299 hourly, moving 24h-mean concentrations; r = 0.72 for hourly concentrations). The modeled biomass
300 combustion PM may constitute a considerable fraction of the total PM2.5 during some episodes. The
301 average modeled biomass carbonaceous PM during the period is about 1.3 μg m^{-3}, which is about 12%
302 of the average measured PM2.5 concentration (11 μg m^{-3}).

303 The measured K and particle number concentrations in the two combustion-related
304 components (Clusters 1 and 2) are also compared to the results from the EMEP MSC-W model
305 simulations. Since K is not explicitly modeled the comparison is based on model results for other
306 particulate components that can be tracked to different source types. Model results for primary
307 emitted fine particles (PPM2.5) from anthropogenic sources and open fires are used (Figures 13 and
308 14). The modeled PPM2.5 is split into PPM2.5 from (i) residential biomass combustion, (ii) open
309 vegetation fires (including both wildfires and agricultural burning), and (iii) other anthropogenic
310 sources (predominantly fossil fuel sources).

311 Figure 13 shows a comparison between modeled concentrations of PPM2.5 from biomass
312 combustion (residential + open fires) and the measured K concentration in cluster 1. Overall the
313 modeled concentrations show a high degree of correlation with experimental data. The main
314 exception is a cold and windy 6-day period in February, where the model produces significantly
315 lower values (for the first five days). The meteorological conditions during this period result in a
316 high demand for local residential heating, and we attribute this discrepancy to an underestimation
317 of contributions from local sources – the total PM2.5 concentrations at the urban background station
318 Femman were low during the first four days of the "cluster 1 episode", and this indicates that
319 source(s) of the elevated K-concentrations measured with the AMS may have been located relatively
320 close to the university site and possibly only impacting a relatively small area; the wind direction
321 was rather stable during the whole episode. Local episodes of this type are difficult to model
322 accurately with a large scale chemical transport models due to the low spatial resolution of the
323 model simulations and emission data. The model simulations also confirm the importance of
324 contributions from open fires, in particular, agricultural burns, in late March (compare with Figs. 8
325 and 9).

326 Figure 14 illustrates the modeled concentration of PPM2.5 from fossil fuel combustion and the
327 measured K concentration in cluster 2. The correlation between the model and measurements is
328 lower for cluster 2 than for cluster 1 — this is not surprising since the model PPM2.5 (from other
329 sources than biomass burning) represents sums of many different sources, and the K emissions are
330 likely to be different for different emission sources. However, several features in the experimental
331 data are qualitatively represented by the model results.

332 A separate set of model simulations were performed to investigate the correlation between the
333 AMS measurements and individual primary particle emission categories. The correlation
334 coefficients between measured concentrations and modeled PPM2.5 from different emission sources
335 are given in Table 2. The measured concentrations in cluster 1 are most strongly correlated with
336 modeled biomass combustion particles, with a maximum r = 0.76 observed for total PPM2.5 from
337 biomass combustion (residential combustion + open biomass burning). The correlation with
338 modeled fossil fuel components is relatively low. In general, modeled concentrations are somewhat
339 better correlated with measured number concentrations than with K concentrations. Although the
340 measured Na concentrations are very low in cluster 1, the correlation (not shown) between these and
341 the modeled concentrations are as good as for K for most components. Based on the relatively high
342 correlations observed, we conclude that the cluster 1 particles observed with the Alkali AMS are
343 mainly emitted from biomass combustion.

344 The correlation coefficients between the measured concentrations in Cluster 2 and various
345 model components are also given in Table 2. Cluster 2 corresponds less well to any modeled
346 compound than cluster 1 does; the highest correlations are found for emissions from the

347   Agricultural sector (SNAP-10; not including Open Burning of Biomass, r=0.65 when compared with
348   the cluster 2 number concentration) and for the sum of all "non-biomass" emission sources (r = 0.63).
349   Correlation is especially low for particles from residential biomass combustion (r < 0.23). This
350   indicates that cluster 2 is at least not dominated by particles from residential biomass combustion in
351   the region around Gothenburg. For cluster 2 the correlation coefficients are similar for particle
352   number and K concentrations, while they are lower for Na concentrations (not shown; r < 0.36 for all
353   model components in Table 2 except for residential/non-industrial fossil fuel combustion, for which
354   r=0.61 for Na in cluster 2). The lower correlations for Na have not been studied in detail, but one
355   possible explanation may be interference from sea salt particles at the defined border between
356   Cluster 2 and 3 (see Fig. 1).

357   To investigate if emissions from any single geographical region could be responsible for a large
358   fraction of the cluster 2 particles, simplified model simulations, that track primary particle emissions
359   from a number of areas in Europe (Sweden, Norway, Poland/Czech/Slovakia [PCS], Eastern Europe
360   [EEU = Russia, Belarus, the Baltic states, Finland, Ukraine] and Western Europe [WEU = Denmark,
361   Germany, BeNeLux, France], the British Isles [UK, Ireland]), were performed with the EMEP
362   MSC-W model. These simulations indicated that different cluster 2 peaks correspond to different
363   source regions; no single region seems to dominate cluster 2. The highest measured concentrations
364   in cluster 2 (late April) seem to be associated with air masses from Western Europe. The broad peak
365   at the end of March is associated with air from Eastern Europe and for the later part also with more
366   southerly air that has passed Poland and other parts of Central Europe; Swedish emissions also
367   influenced Gothenburg during this period. Several other peaks can be related to emissions in PCS,
368   WEU, EEU, and Sweden.

369   We conclude that Cluster 2 seems to represent emissions from different emission sources and
370   regions that contribute to the air quality in Gothenburg by long-range transport.

371   *3.5 Comparison with earlier studies*

372   The present results agree with measurements performed in Gothenburg during 2003 and 2004
373   with the Alkali AMS that only monitored one type of alkali ion at the time [29]. Mass concentrations
374   of alkali in ambient air varied in the range 0.02–100 ng m^{-3} and the number of alkali-containing
375   particles varied between 0.1 and 100 cm^{-3}. The detected aerosol was concluded to be dominated by
376   emissions from combustion of biomass and fossil fuels, with a significant contribution from sea-salt
377   particles only during intrusion of marine air.

378   A long term measurement of Na and K in an urban and marine environment by Ooki *et al*. [57]
379   reported an average K:Na ratio of 1.8 for the fine particles (D < 1.1 μm), the study concluded that the
380   primary source of the fine particles was a domestic refuse incineration plant located within 15 km of
381   the measurement site. This finding, K:Na ratio of 1.8, by Ooki *et al*. [57] agrees with the K:Na ratio of
382   1.2–1.7 reported by Mamane [58] from the direct household refuse incinerator aerosol measurements
383   with the fine particles (D < 2.5 μm). In the present work, the air masses originating from western
384   Europe (W) had an average K:Na value of 2.2, which may suggest the emissions were associated
385   with refuse combustions. A slightly higher value of K:Na than Mamane [58] can be explained by
386   different combusted source materials. In European countries, the usage of both small and large scale
387   biomass burning systems are common; especially during the cold winter period, usage of domestic
388   heating systems with biomass fuel may contribute to the higher K:Na ratio.

389   Stohl *et al*. [59] reported measurements of Arctic air pollution due to biomass burning
390   associated with agricultural fire activities in Eastern Europe during the spring; this type of fire
391   smoke can reach the Arctic region and potentially reduce the snow albedo and change the rate of
392   snow/ice melting. The filter samples from the Zeppelin mountain station in Svalbard indicated
393   elevated concentrations of levoglucosan, K, and CO for the biomass burning pollution events from
394   April 27 to May 9, 2006. These results suggest that the monitoring of K and CO can be used as a good
395   indicator for the potential contribution of air pollution from biomass burning in the Arctic region.
396   Since the SI-AMS has single-particle analysis capability, it has further potential to obtain more
397   detailed information.

4. Conclusions

Aerosol mass spectrometry has been used to measure the K and Na concentrations in submicron particles in Gothenburg, Sweden, during winter and spring seasons. Typical PM1 alkali concentrations were in the range from 1–50 ng m^{-3}, but with large variations in concentrations and Na:K ratio depending on the prevailing conditions. High concentrations of Na-containing particles were favored by westerly winds and high wind speeds and were concluded to be related to sea salt particles in marine air masses. High concentrations of K-containing particles correlated with low temperatures and low wind speeds and were mainly related to regional emissions and transport of air masses originating from continental Europe. Low Na:K ratios suggested that these particles originated from solid fuel combustion, including biomass burning. Diurnal variations in both K and Na concentrations were observed during a springtime period with daily temperature inversions. The K-rich particles were to a large extent transported from areas with extensive agricultural burns in Eastern Europe during the beginning of this period, during the later part residential biomass combustion emissions also made significant contributions. Further development and application of the methodology presented in this study, including analysis of single particle data may improve the ability to distinguish particles from different sources. To implement any regulatory approach to improve air quality, one needs to have a clear understanding of the emission sources. Alkali-AMS measurements can be a useful tool to identify contributions from biomass burning emissions to submicron particulate matter.
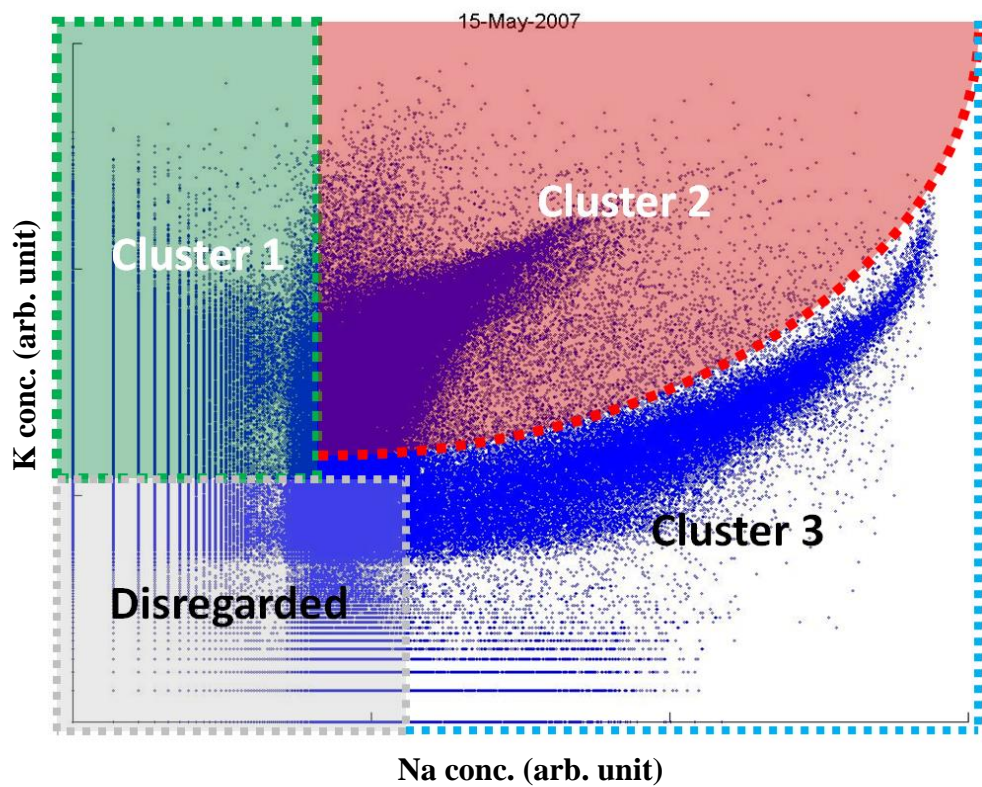
417
418
419
420
421
422
423
424
425
426
427
428
429
430
431

432 **Figure 1.** Cluster boundaries in logarithmic scale, where the boundaries were defined based on
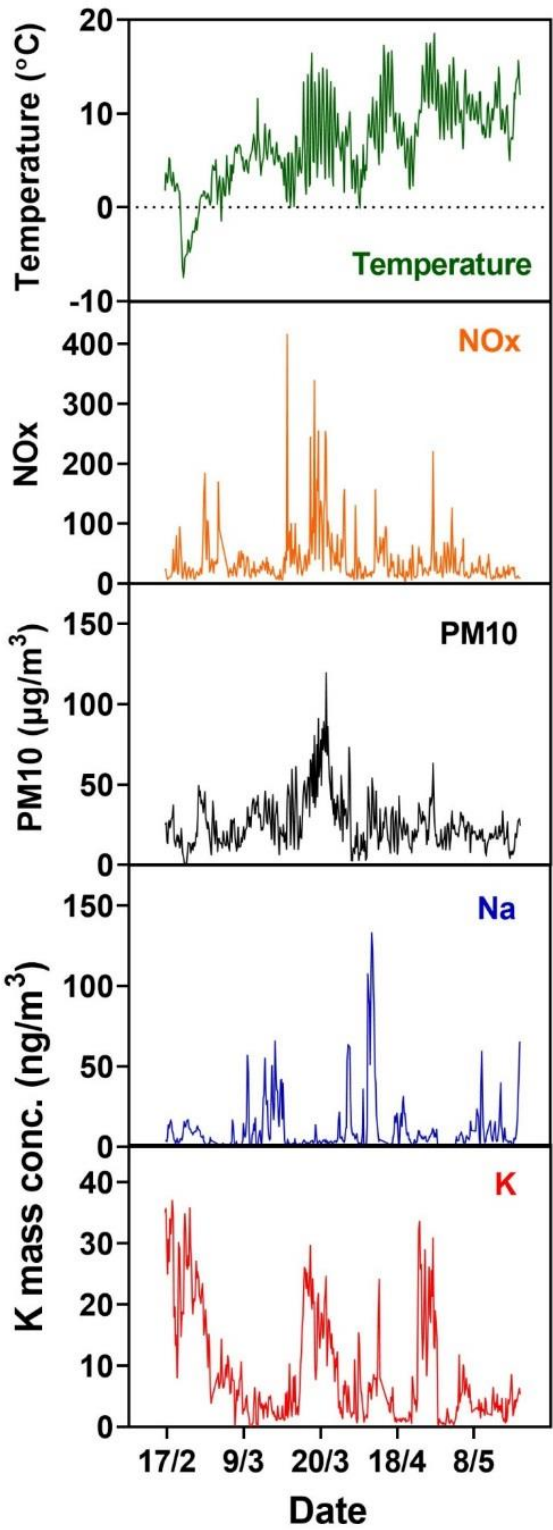433 clustering analysis of Na and K content of individual aerosol particles.

434
435
436
437
438
439
440
441
442
443
444
445
446
447
448
449
450
451
452
453
454
455
456
457
458

Figure 2. Concentrations of Na and K in submicron particles as a function of time measured by the Alkali AMS, together with temperature, and PM10 and NOx concentrations measured at the Femman station. Displayed values are averages over 6 min intervals.
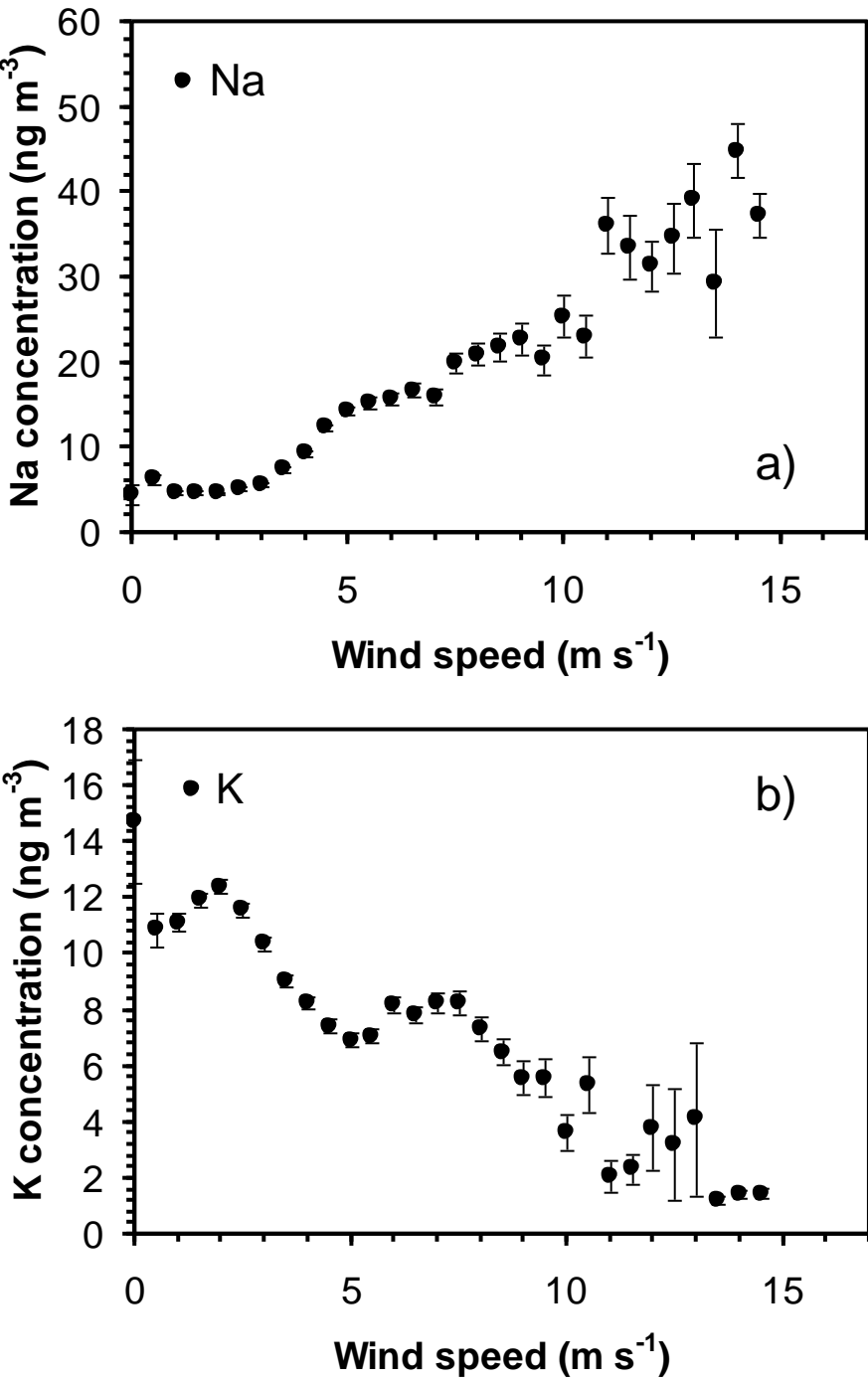
Figure 3. Concentrations of Na and K in Clusters 1–3 as a function of time. Displayed values are averages over 6 min intervals. Cluster 1 is associated with residential biomass combustion, Cluster 2 with multiple combustion sources, and Cluster 3 with sea salt in marine aerosol. See text for further details about the analysis and interpretation of Clusters 1–3.

488

489
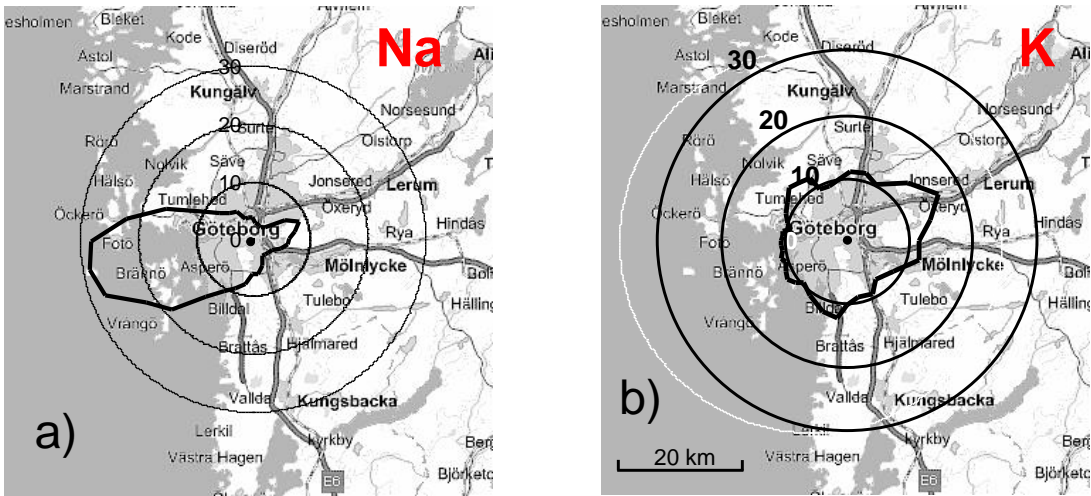
490   **Figure 4.** a) Na and b) K concentrations as a function of wind direction (Femman station) for all data
491   obtained during the measurement campaign.

Figure 5. a) Na and b) K concentrations as a function of temperature for all data obtained during the measurement campaign. Error bars correspond to ±1 standard error.
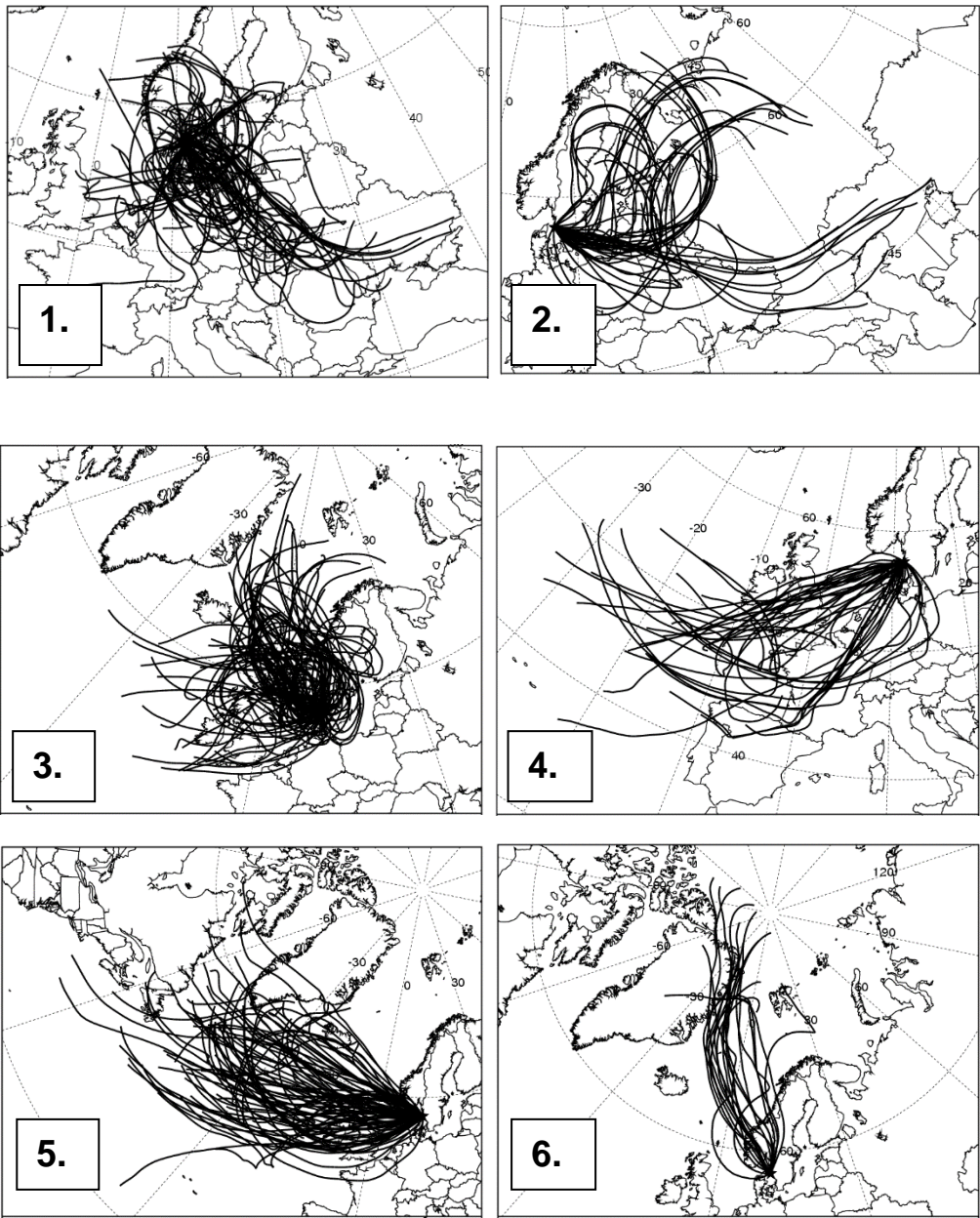
Figure 6. Back trajectory group analysis for six air mass types reaching Gothenburg during the period from 16 February 00:00 to 21 May 00:00 mean trajectories (uppermost panel), and individual trajectories attributed to the six groupings: C, E, N, W, A, and P. The traces correspond to 72 h backward trajectories calculated using the HYSPLIT4 model (Draxler and Hess, 2004). New trajectories were started every 6 h and ended 500 m above ground level in Gothenburg.
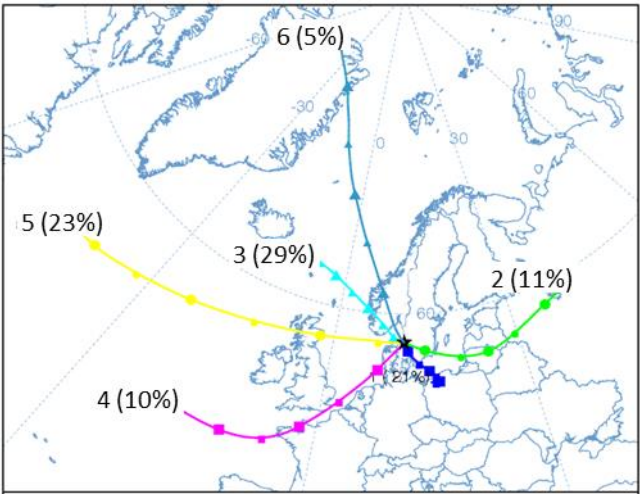
557

558

559

560

561

562

563

564

565

566

567

568   **Figure 7.** Mean back trajectories based on the group analysis illustrated in Figure 6. The six groups
569   and percent of the total number of trajectories assigned to each group are indicated. See text for
570   further details.

571

572

573

574

575

576

577

578

579

580

581

582

583

584

585

586
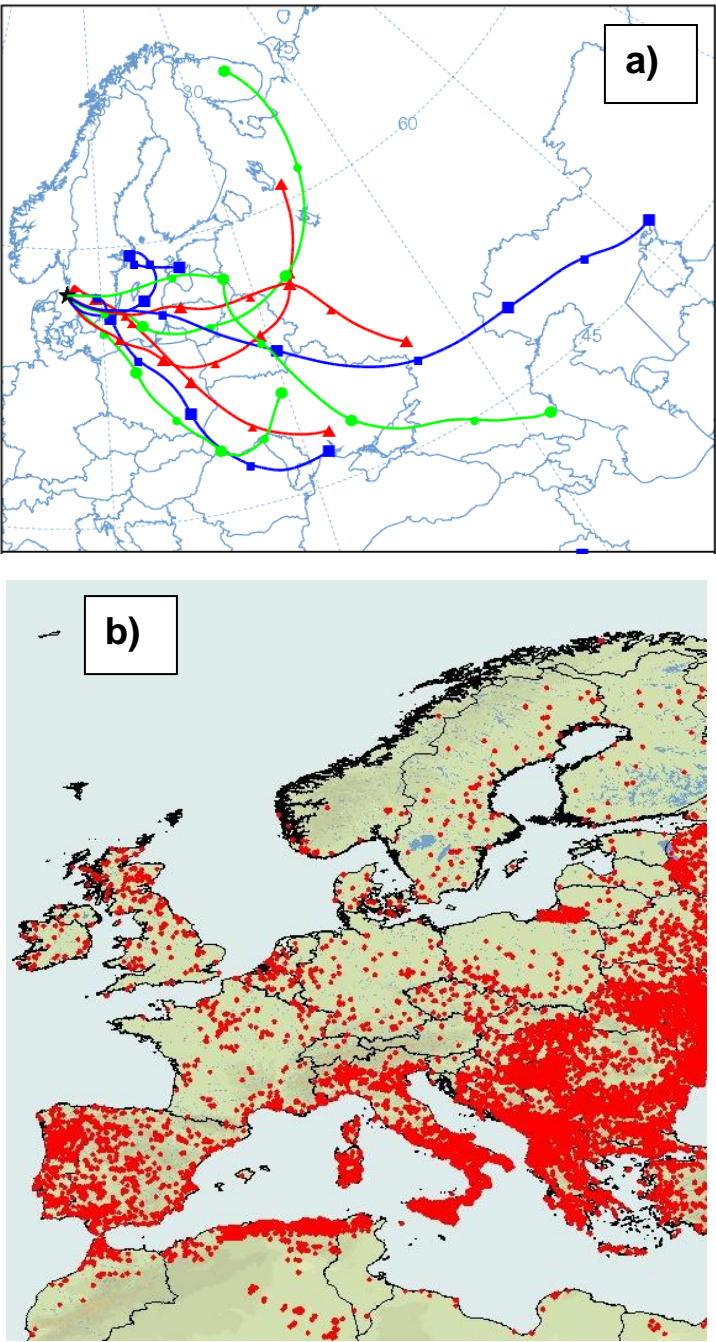
587

588

589

590

591

592   **Figure 8.** a) 72 h backward trajectories for the same period. A new trajectory was started every 12 h. b)
593   Distribution of fires from March 24 to April 1, 2007. Each dot on the map indicates a fire detected
594   with the moderate resolution imaging spectroradiometer (MODIS) aboard the Terra satellite (Roy et
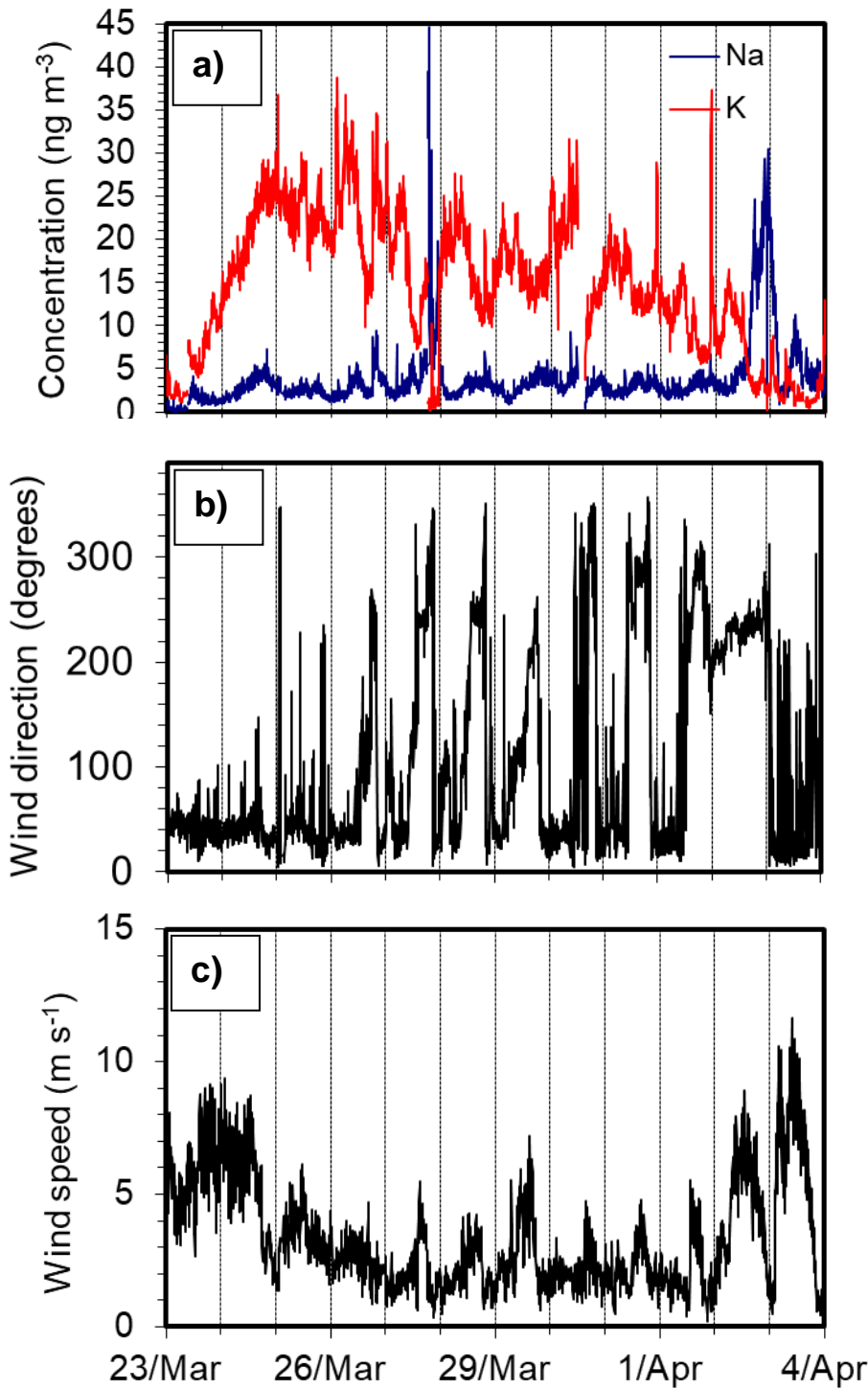595   al., 2002).

Figure 9. Experimental data from an episode from March 24 to April 4 with high K concentrations: a) K and Na concentrations, b) wind direction, and c) wind speed.
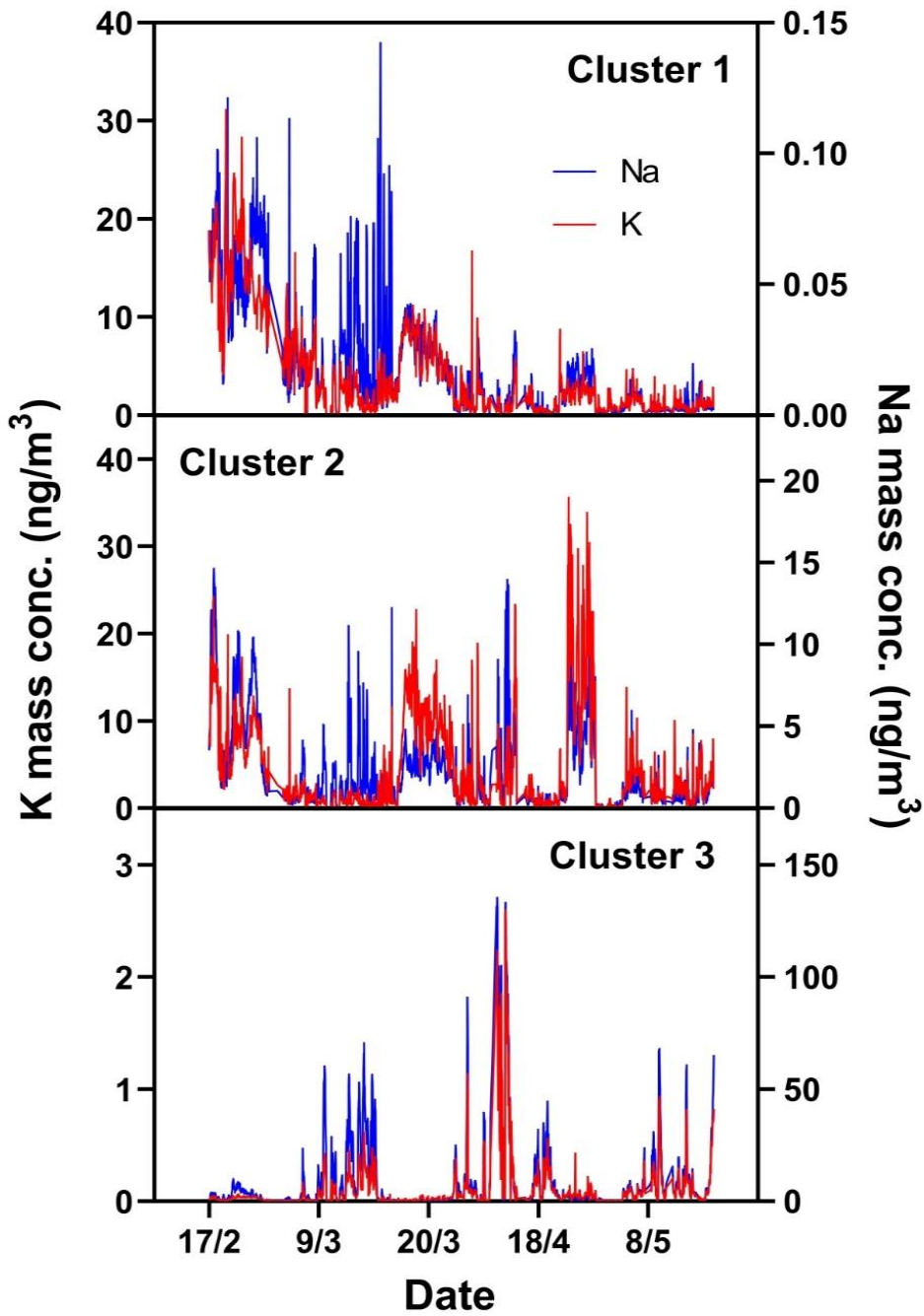
621

622

623

624

Figure 10. K concentration in Clusters 1 and 2 as a function of a) temperature, b) wind speed, and c) wind direction.

627

628

629

630

631

632

633

634

635

636

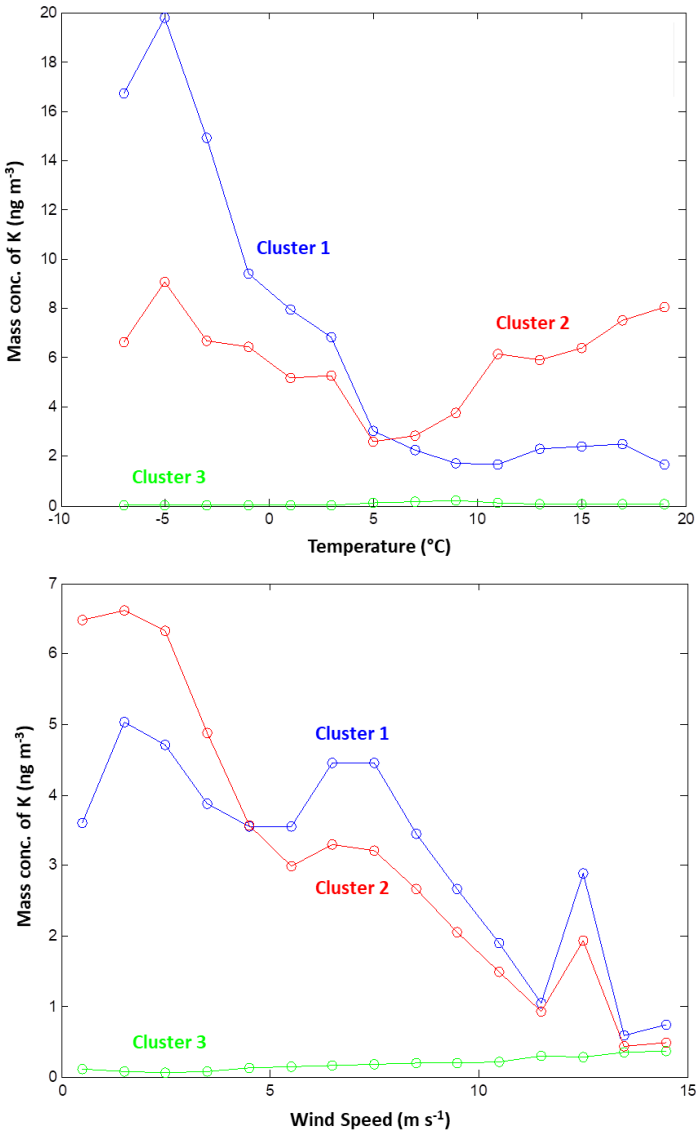637

638

639

640

641

642

643

644

645

646 **Figure 11.** Measured PM2.5-concentrations at the urban background station Femman in Gothenburg
647 (black line, right scale), during the period 17 Feb. – 20 May 2007, and modeled concentrations of
648 particulate carbonaceous matter (PCM) in PM2.5 from: residential biomass combustion (grey, dashed
649 line), open biomass burning fires (including wild fires and agricultural fires; orange line), and total
650 biomass burning PCM (red line). Unit: μg m^{-3}. The data have been smoothed using moving 24 h
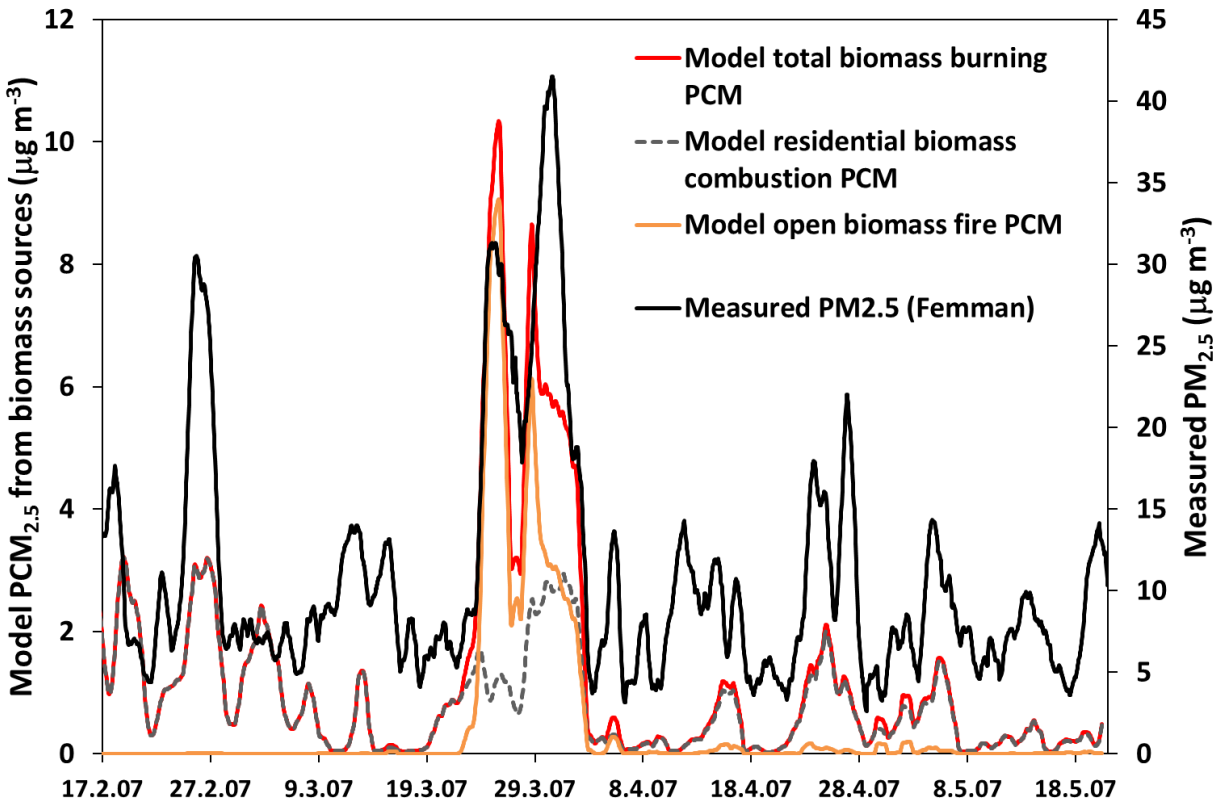651 mean concentrations.

652

653

654

Figure 12. Comparison of the modeled hourly concentrations of primary PM2.5 from residential biomass combustion (blue line) and open fires (red line) and measured (hourly average) concentrations of K in Cluster 1 (black line). Units, model results: ng m^{-3}; measurements: ng K m^{-3}.

658

659

660   **Figure 13.** Comparison of the modeled hourly concentrations of primary PM2.5 from fossil fuel
661   combustion (red line) and measured (hourly average) concentrations of K in cluster 1 (black line).
662   Units, model results: $\mu g\ m^{-3}$; measurements: ng K m^{-3}.
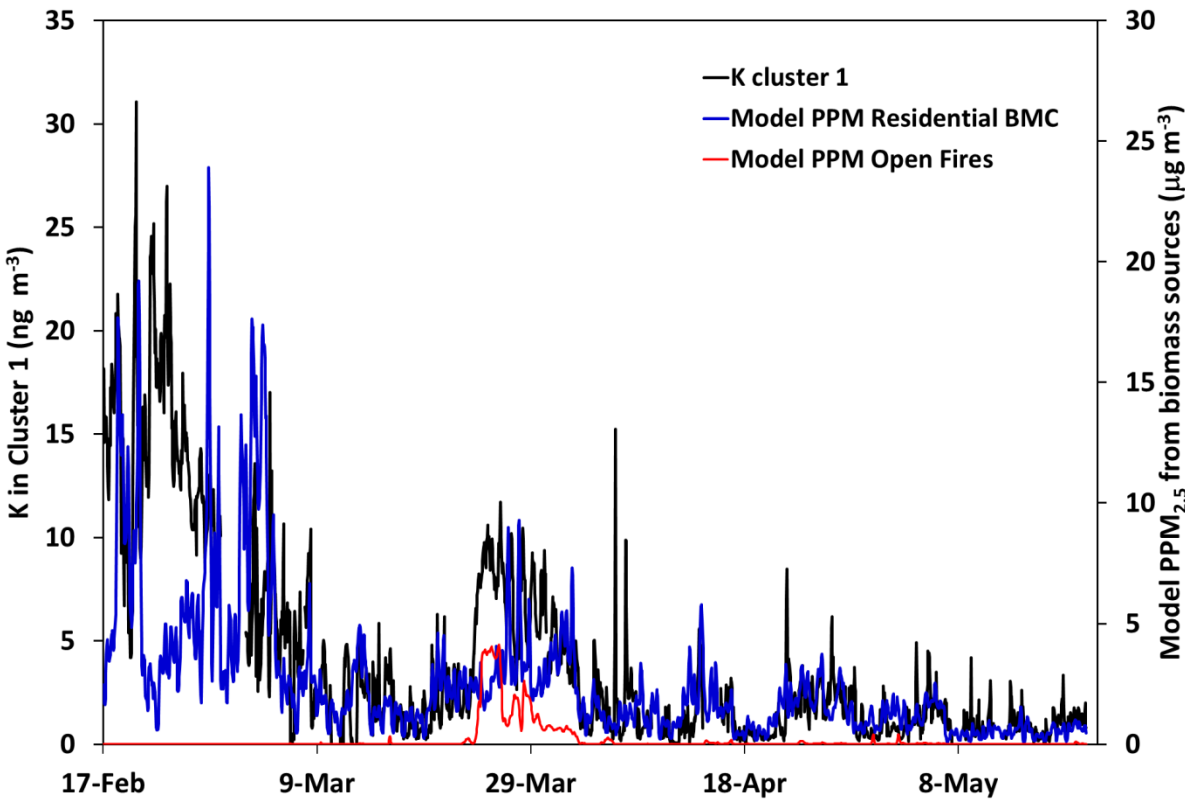
663

664

665   **Figure 14.** Comparison of the modeled hourly concentrations of primary PM2.5 from fossil fuel
666   combustion (red line) and measured (hourly average) concentrations of K in cluster 2 (black line).
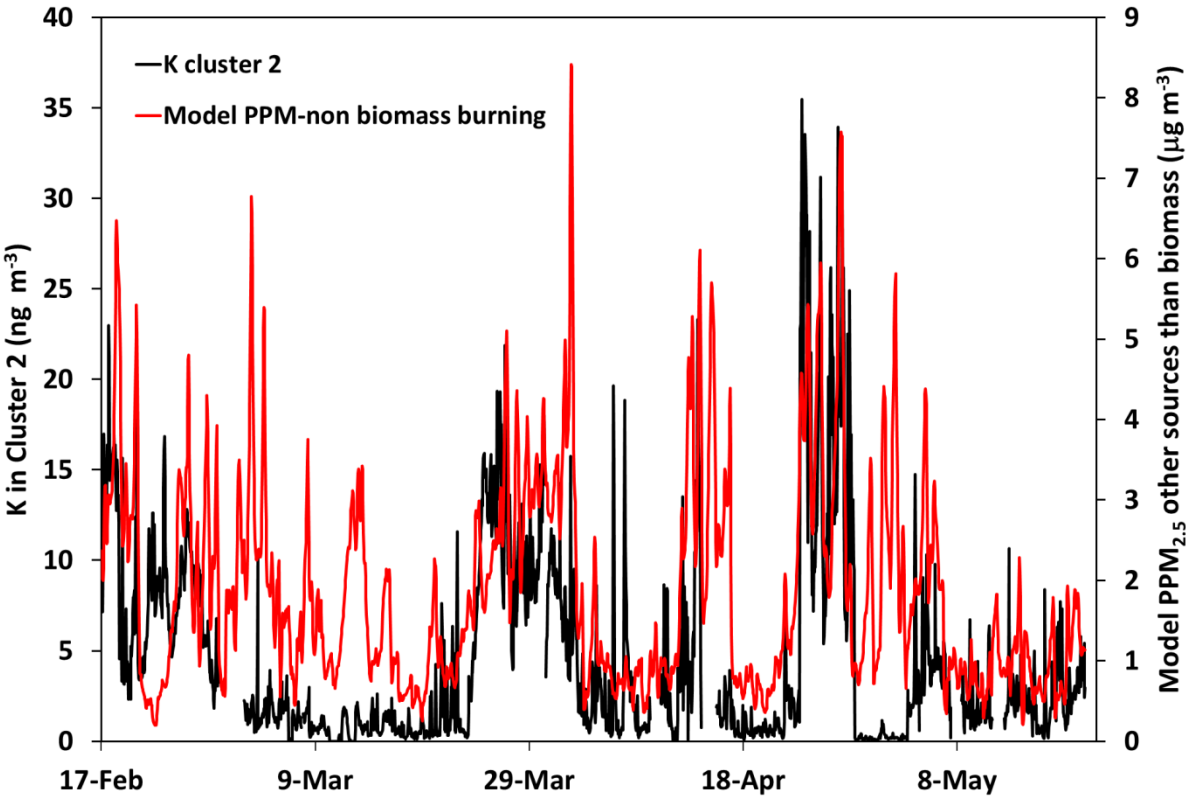667   Units, model results: μg m⁻³; measurements: ng K m⁻³.

668 **Table 1.** Back trajectory group analysis for six air mass types indicates the air mass category, number of 6 min.

669 samples, percent of the total number of trajectories assigned to each group, mean Na and K concentrations [ng

670 m^{-3}], Na:K concentration ratio, mean PM$_{10}$ and trace gas concentrations [μg m^{-3}], temperature (T) [°C] and wind

671 speed (WS) [m s^{-1}].

672

Origin group (Initial)	Samples	%	Na	K	Na/K	PM10	O$_3$	NO	NOx	T	WS
1. Central Eur. (C)	3238	19	3.9	14	0.27	34.8	46.2	11.5	51.4	7.0	3.5
2. Eastern Eur. (E)	2171	13	6.2	21	0.29	34.1	53.8	16.6	57.6	2.9	4.7
3. Northern Eur.(N)	5027	30	6.0	5.6	1.1	20.1	57.6	7.8	36.0	8.3	3.5
4. Western Eur. (W)	1393	8	4.9	11	0.45	25.3	49.3	4.6	32.0	8.0	3.6
5. Atlantic (A)	4188	25	33	3.6	9.2	27.2	66.6	2.7	23.3	7.2	5.4
6. Polar (P)	847	5	8.6	2.7	3.2	20.1	57.1	9.1	36.9	4.9	4.7

673

674 **Table 2.** Correlation coefficients (r) between measured concentrations in cluster 1 and 2 (particle number and K
675 mass concentrations) and modeled concentrations of particulate matter from primary emissions (PPM) from
676 selected sources; both measured and modeled concentrations were smoothed using 24-h moving average
677 concentrations. Correlation coefficients with values above 0.5 are marked in bold.

678

Model tracer compound/source category	correlation coefficient (r)			
	Cluster 1 Number	Cluster 1 K	Cluster 2 Number	Cluster 2 K
Total Biomass Burning (residential + fires)	**0.76**	**0.64**	0.24	0.31
Residential Biomass Combustion (SNAP-2)	**0.71**	**0.62**	0.15	0.23
Open Biomass Burning (Fires)	0.38	0.21	0.44	0.41
Total Other Anthropogenic PPM sources[a]	0.41	0.26	**0.63**	**0.61**
Non-industrial/residential combustion fossil fuels (coal, oil, gas) (SNAP-2)	**0.51**	**0.54**	0.27	0.37
Manufacturing industry (SNAP-3)	**0.53**	0.30	**0.61**	**0.58**
Road transport (SNAP-7)	0.39	0.19	**0.57**	**0.52**
International shipping	-0.04	-0.08	0.33	0.30
Other mobile sources/machinery	0.28	0.12	**0.53**	0.50
Agriculture (SNAP-10)	0.33	0.12	**0.65**	**0.59**

679 [a] Includes all anthropogenic primary PM sources, except residential biofuel combustion and Open Biomass
680 Burning (Fires) – this is expected to be mainly from fossil fuel sources.
681

696   ## References

697   1.   Chen, J.; Li, C.; Ristovski, Z.; Milic, A.; Gu, Y.; Islam, M.S.; Wang, S.; Hao, J.; Zhang, H.; He, C.; Guo,
698   H.; Fu, H.; Miljevic, B.; Morawska, L.; Thai, P.; LAM, Y.F.; Pereira, G.; Ding, A.; Huang, X.; Dumka,
699   U.C. A review of biomass burning: Emissions and impacts on air quality, health and climate in China,
700   *Sci. Total Environ.* **2017**, *579*, 1000-1034.
701   2.   Kelly, F. J.; and Fussell, J. C. Size, source and chemical composition as determinants of toxicity
702   attributable to ambient particulate matter, *Atmos. Environ.* **2012**, *60*, 504–526.
703   3.   Lee, A.; Kinney, P.; Chillrud, S.; Jack, D. A Systematic Review of Innate Immunomodulatory Effects of
704   Household Air Pollution Secondary to the Burning of Biomass Fuels, *Ann. Glob. Health* **2015**, *81*,
705   368-74.
706   4.   Deering-Rice, C.E.; Nguyen, N.; Lu, Z.; Cox, J.E.; Shapiro, D.; Romero, E.G.; Mitchell, V.K.; Burrell,
707   K.L.; Veranth, J.M.; Reilly, C.A. Activation of TRPV3 by Wood Smoke Particles and Roles in
708   Pneumotoxicity, *Chem. Res. Toxicol.* **2018**, *31*, 291–301.
709   5.   Scott, A.F.; Reilly, C.A. Wood and Biomass Smoke: Addressing Human Health Risks and Exposures,
710   *Chem. Res. Toxicol.,* **2019**, 18;32(2):219–221. doi: 10.1021/acs.chemrestox.8b00318.
711   6.   Viana, M.; Kuhlbusch, T. A. J.; Querola, X.; Alastueya, A.; Harrison, R. M.; Hopke, P. K.; Winiwarter,
712   W.; Vallius, M.; Szidat, S.; Prévôt, A. S. H.; Hueglin, C.; Bloemen, H.; Wåhlin, P.; Vecchi, R.; Miranda,
713   A. I.; Kasper-Giebl, A.; Maenhaut, W.; Hitzenberger, R. Source apportionment of particulate matter in
714   Europe: A review of methods and results, *Aerosol Sci.* **2008**, *39*, 827–849.
715   7.   Andersen, Z. J.; Wåhlin, P.; Raaschou-Nielsen, O.; Scheike, T.; Loft, S. Ambient particle source
716   apportionment and daily hospital admissions among children and elderly in Copenhagen, *J. Expo. Sci.*
717   *Environ. Epidemiol.* **2007**, *17*, 625–636.
718   8.   Denier van der Gon, H. A. C.; Bergström, R.; Fountoukis, C.; Johansson, C.; Pandis, S. N.; Simpson, D.
719   & Visschedijk, A. J. H. Particulate emissions from residential wood combustion in Europe - revised
720   estimates and an evaluation, *Atmos. Chem. Physics* **2015**, 6503-6519.
721   9.   Glasius, M.; Hansen, A.; Claeys, M.; Henzing, J.; Jedynska, A.; Kasper-Giebl, A.; Kistler, M.;
722   Kristensen, K.; Martinsson, J.; Maenhaut, W.; Nøjgaard, J.; Spindler, G.; Stenström, K.; Swietlicki, E.;
723   Szidat, S.; Simpson, D.; Yttri, K. Composition and sources of carbonaceous aerosols in Northern
724   Europe during winter, *Atmos. Environ.* **2018**, *173*, 127-141.
725   10.   Szidat, S.; Jenk, T. M.; Synal, H.-A.; Kalberer, M.; Wacker, L.; Hajdas, I.; Kasper-Giebl, A.;
726   Baltensperger, U. Contributions of fossil fuel, biomass burning, and biogenic emissions to
727   carbonaceous aerosols in Zürich as traced by 14C, *J. Geophys. Res.* **2006**, *111*, D07206.
728   11.   Szidat, S.; Prévôt, A. S. H.; Sandradewi, J.; Alfarra, M. R.; Synal, H.-A.; Wacker, L.; Baltensperger, U.
729   Dominant impact of residential wood burning on particulate matter in Alpine valleys during winter,
730   *Geophys. Res. Lett.* **2007**, *34*, L05820.
731   12.   Szidat, S.; Ruff, M.; Wacker, L.; Synal, H. A.; Hallquist, M.; Shannigrahi, A. S.; Yttri, K. E.; Dye, C.;
732   Simpson, D. Fossil and non-fossil sources of organic carbon (OC) and elemental carbon (EC) in
733   Göteborg, Sweden, *Atmos. Chem. Phys.* **2009**, *9*, 1521-1535.

734   13.   Simoneit, B. R. T. Biomass Burning — a Review of Organic Tracers for Smoke from Incomplete
735   Combustion, *Appl. Geochem.* **2002**, *17*, 129-162.
736   14.   Elsasser, M.; Crippa, M.; Orasche, J.; DeCarlo, P. F.; Oster, M.; Pitz, M.; Cyrys, J.; Gustafson, T. L.;
737   Pettersson, J. B. C.; Schnelle-Kreis, J.; Prévôt, A. S. H.; Zimmermann R. Organic molecular markers
738   and signature from wood combustion particles in winter ambient aerosols: aerosol mass spectrometer
739   (AMS) and high time-resolved GC-MS measurements in Augsburg, Germany, *Atmos. Chem. Phys.*
740   **2012**, *12*, 6113-6128.
741   15.   Tao, J.; Zhang, L. M.; Zhang, R. J.; Wu, Y. F.; Zhang, Z. S.; Zhang, X. L.; Tang, Y. X.; Cao, J. J.; Zhang, Y.
742   H. Uncertainty Assessment of Source Attribution of PM2.5 and its Water-soluble Organic Carbon
743   Content using Different Biomass Burning Tracers in Positive Matrix Factorization Analysis - a Case
744   Study in Beijing, China, *Sci. Total Environ.* **2016**, *543*, 326-335.
745   16.   Fourtziou, L.; Liakakou, E.; Stavroulas, I.; Theodosi, C.; Zarmpas, P.; Psiloglou, B.; Sciare, J.; Maggos,
746   T.; Bairachtari, K.; Bougiatioti, A.; Gerasopoulos, E.; Sarda-Esteve, R.; Bonnaire N.; Mihalopoulos N.
747   Multi-tracer Approach to Characterize Domestic Wood Burning in Athens (Greece) during
748   Wintertime, *Atmos. Environ.* **2017**, *148*, 89-101.
749   17.   Nielsen, I. E.; Eriksson, A. C.; Lindgren, R.; Martinsson, J.; Nystrom, R.; Nordin, E. Z.; Sadiktsis, I.;
750   Boman, C.; Nojgaard J. K.; Pagels J. Time-resolved Analysis of Particle Emissions from Residential
751   Biomass Combustion Emissions of Refractory Black Carbon, PAHs and Organic Tracers, *Atmos.*
752   *Environ.* **2017**, *165*, 179-190.
753   18.   Achad, M.; Caumo, S.; Vasconcellos, P. D.; Bajano, H.; Gomez D.; Smichowski P. Chemical Markers of
754   Biomass Burning: Determination of Levoglucosan, and Potassium in Size-classified Atmospheric
755   Aerosols Collected in Buenos Aires, Argentina by Different Analytical Techniques, *Microchem. J.* **2018**,
756   *139*, 181-187.
757   19.   Rad, F. M.; Spinicci, S.; Silvergren, S.; Nilsson U.; Westerholm R. Validation of a HILIC/ESI-MS/MS
758   Method for the Wood Burning Marker Levoglucosan and its Isomers in Airborne Particulate Matter,
759   *Chemosphere* **2018**, *211*, 617-623.
760   20.   Heringa, M. F.; DeCarlo, P. F.; Chirico, R.; Lauber, A.; Doberer, A.; Good, J.; Nussbaumer, T.; Keller,
761   A.; Burtscher, H.; Richard, A.; Miljevic, B.; Prevot A. S. H.; Baltensperger, U. Time-Resolved
762   Characterization of Primary Emissions from Residential Wood Combustion Appliances, *Environ. Sci.*
763   *Tech.* **2012**, *46*, 11418-11425.
764   21.   Elsasser, M.; Busch, C.; Orasche, J.; Schön, C.; Hartmann, H.; Schnelle-Kreis J.; Zimmermann R.
765   Dynamic Changes of the Aerosol Composition and Concentration during Different Burning Phases of
766   Wood Combustion, *Energy & Fuels* **2013**, 27, 4959-4968.
767   22.   Suess, D. T.; Prather, K. A. Mass Spectrometry of Aerosols. *Chem. Rev.* **1999**, *99*, 3007.
768   23.   Johnston, M. V. Sampling and Analysis of Individual Particles by Aerosol Mass Spectrometry, *J. Mass.*
769   *Spectrom.* **2000**, *35*, 585–595.
770   24.   Noble, C. A.; Prather, K. A.; Real-time single particle mass spectrometry: A historical review of a
771   quarter century of the chemical analysis of aerosols, *Mass Spectrom. Rev.* **2000,** 19, 248–274.
772   25.   Coe, H.; Allan, J. D.; Alfarra, M. R.; Bower, K. N.; Flynn, M. J.; McFiggans, G. B.; Topping, D.
773   O.; Williams, P. I.; O'Dowd, C. D.; Dall'Osto, M.; Beddows, D. C. S.; Harrison, R. M. Chemical and
774   physical characteristics of aerosol particles at a remote coastal location, Mace Head, Ireland, during
775   NAMBLEX, *Atmos. Chem. Phys*. **2006**, *6*, 3289-3301.
776   26.   Canagaratna, M. R.; Jayne, J. T.; Jimenez, J. L.; Allan, J. D.; Alfarra, M. R.; Zhang, Q.; Onasch, T. B.;
777   Drewnick, F.; Coe, H.; Middlebrook, A.; Delia, A.; Williams, L. R.; Trimborn, A. M.; Northway, M. J.;
778   DeCarlo, P. F.; Kolb, C. E.; Davidovits, P.; Worsnop, D. R. Chemical and microphysical
779   characterization of ambient aerosols with the aerodyne aerosol mass spectrometer, *Mass Spectrom. Rev.*
780   **2007,** 26, 185–222.
781   27.   Svane, M.; Hagström, M.; and Pettersson, J. B. C. Chemical Analysis of Individual Alkali-Containing
782   Aerosol Particles: Design and Performance of a Surface Ionization Particle Beam Mass Spectrometer,
783   *Aerosol Sci. Technol.* **2004**, *38*, 655–663.
784   28.   Svane, M. Gustafsson, T. L.; Kovacevik, B.; Noda, J.; Andersson, P. U.; Nilsson, E. D.; Pettersson, J. B.
785   C. On-line chemical analysis of individual alkali-containing aerosol particles by surface ionization
786   combined with time-of-flight mass spectrometry, *Aerosol Sci. Technol.* **2009**, *43*, 453-661.

787   29. Svane, M.; Janhäll, S.; Hagström, M.; Hallquist, M.; and Pettersson, J. B. C. On-line Alkali Analysis of
788   Individual Aerosol Particles in Urban Air, *Atmos. Environ.* **2005a**, *39*, 6919–6930.

789   30. Svane, M.; Hagström, M.; and Pettersson, J. B. C. Online Measurements of Individual
790   Alkali-Containing Particles Formed in Biomass and Coal Combustion: Demonstration of an
791   Instrument Based on Surface Ionization Technique, *Energy & Fuels.* **2005b**, *19*, 411–417.

792   31. Svane, M.; Hagström, M.; Davidsson K. O.; Boman, J.; and Pettersson, J. B. C. Cesium as a Tracer for
793   Alkali Processes in a Large-scale Combustion Facility. *Energy & Fuels* **2006**, *20*, 979–985.

794   32. Hu, Q.H.; Xie, Z.Q.; Wang, X.M.; Kang, H.; and Zhang,P. Levoglucosan indicates high levels of
795   biomass burning aerosols over oceans from the Arctic to Antarctic. *Sci. Rep.* **2013**, *3*, 3119.

796   33. Pratap, V.; Chen, Y.; Yao, G.; and Nakao, S.; Temperature effects on multiphase reactions of organic
797   molecular markers: A modeling study, *Atmos. environ.* **2018**, *179*, 40–48.

798   34. Simpson, D.; Benedictow, A.; Berge, H.; Bergström, R.; Emberson, L. D.; Fagerli, H.; Flechard, C. R.;
799   Hayman, G. D.; Gauss, M.; Jonson, J. E.; Jenkin, M. E.; Nyíri, A.; Richter, C.; Semeena, V. S.; Tsyro, S.;
800   Tuovinen, J.-P.; Valdebenito, Á.; Wind, P. The EMEP MSC-W chemical transport model – technical
801   description, *Atmos. Chem. Phys.* **2012**, *12*, 7825–7865.

802   35. Liu, P.; Ziemann, P. J.; Kittelson, D. B.; McMurry, P. H. Generating Particle Beams of Controlled
803   Dimensions and Divergence: I. Theory of Particle Motion in Aerodynamic Lenses and Nozzle
804   Expansions, *Aerosol Sci. Technol.* **1995a**, *22*, 292–313.

805   36. Liu, P.; Ziemann, P. J.; Kittelson, D. B.; McMurry, P. H. Generating Particle Beams of Controlled
806   Dimensions and Divergence: Ii. Experimental Evaluation of Particle Motion in Aerodynamic Lenses
807   and Nozzle Expansions. *Aerosol Sci. Technol.* **1995b**, *22*, 314–324.

808   37. Jayne, J. T.; Leard, D. C.; Zhang, X.; Davidovits, P.; Smith, K. A.; Kolb, C. A.; Worsnop, D. R.
809   Development of an Aerosol Mass Spectrometer for Size and Composition Analysis of Submicron
810   Particles. *Aerosol Sci. Technol.* **2000**, *33*, 49–70.

811   38. Jimenez, J. L.; Jayne, J. T.; Shi, Q.; Kolb, C. A.; Worsnop, D. R.; Yourshaw, I.; Seinfeld, J. H.; Flagan, R.
812   C.; Zhang, X.; Smith, K. A.; Morris, J. W.; Davidovits.; P. Ambient Aerosol Sampling Using the
813   Aerodyne Aerosol Mass Spectrometer, *J. Geophys. Res.* **2003**, *108*, 8425.

814   39. Ionov, N. I. Progress in *Surface Science*. Edited by S G Davison, Oxford: Pergamon Press, 1972; Volume
815   1.

816   40. Zandberg, E. Y. Surface-Ionization Detection of Particles, *Tech. Phys*. **1995**, *40*, 865.

817   41. Ester, M.; Kriegel, H.; Sander, J.; Xu, X. A density-based algorithm for discovering clusters in large
818   spatial databases with noise. Proc .2nd Int. Conf. on Knowledge Discovery and Data Mining, 1996,
819   Portland, OR, 226-231.

820   42. Daszykowski, M.; Walczak, B.; Massart, D.L. Looking for natural patterns in data. Part 1.
821   Density-based approach, *Chemom. Intell. Lab. Syst*. **2001**, *56*, 83-92.

822   43. Draxler, R. R.; Hess, G. D. Description of the HYSPLIT4 modeling system. NOAA Technical
823   Memorandum, 2004, ERL, ARL-224.

824   44. Bergström, R.; Denier van der Gon, H. A. C.; Prévôt, A. S. H.; Yttri, K. E.; and Simpson, D. Modelling
825   of organic aerosols over Europe (2002–2007) using a volatility basis set (VBS) framework: application
826   of different assumptions regarding the formation of secondary organic aerosol, *Atmos. Chem. Phys*.
827   **2012**, *12*, 8499–8527.

828   45. Simpson, D.; Bergström, R.; Tsyro, S. & Wind, P. Updates to the EMEP/MSC-W model, 2018--2019,
829   Transboundary particulate matter, photo-oxidants, acidifying and eutrophying components. EMEP
830   Status Report 1/2019, The Norwegian Meteorological Institute, Oslo, Norway, available at
831   www.emep.int, 145-155.

832   46. Aas, W.; Tsyro, S.; Bieber, E.; Bergström, R.; Ceburnis, D.; Ellermann, T.; Fagerli, H.; Frölich, M.;
833   Gehrig, R.; Makkonen, U.; Nemitz, E.; Otjes, R.; Perez, N.; Perrino, C.; Prévôt, A. S. H.; Putaud, J.-P.;
834   Simpson, D.; Spindler, G.; Vana, M.; and Yttri, K. E.: Lessons learnt from the first EMEP intensive
835   measurement periods, *Atmos. Chem. Phys.* **2012**, *12*, 8073–8094.

836   47. Denier van der Gon, H. A. C.; Bergström, R.; Fountoukis, C.; Johansson, C.; Pandis, S. N.; Simpson, D.;
837   Visschedijk, A. Particulate emissions from residential wood combustion in Europe – revised estimates
838   and an evaluation, *Atmos. Chem. Phys*. **2014**, *14*, 31719–31765.

839   48. Genberg, J.; Denier van der Gon, H. A. C.; Simpson, D.; Swietlicki, E.; Areskoug, H.; Beddows, D.;
840   Ceburnis, D.; Fiebig, M.; Hansson, H. C.; Harrison, R. M.; Jennings, S. G.; Saarikoski, S.; Spindler, G.;

Visschedijk, A. J. H.; Wiedensohler, A.; Yttri, K. E.; Bergström, R. Light-absorbing carbon in Europe – measurement and modelling, with a focus on residential wood combustion emissions, *Atmos. Chem. Phys.* **2013**, *13*, 8719–8738.

49. Jonson, J. E.; Simpson, D.; Fagerli, H.; Solberg, S. Can we explain the trends in European ozone levels?, *Atmos. Chem. Phys.* **2006**, *6*, 51–66.

50. Yttri, K. E.; Simpson, D.; Bergström, R.; Kiss, G.; Szidat, S.; Ceburnis, D.; Eckhardt, S.; Hueglin, C.; Nøjgaard, J. K.; Perrino, C.; Pisso, I.; Prevot, A. S. H.; Putaud, J.-P.; Spindler, G.; Vana, M.; Zhang, Y.-L.; Aas, W. The EMEP Intensive Measurement Period campaign, 2008–2009: characterizing carbonaceous aerosol at nine rural sites in Europe, *Atmos. Chem. Phys.* **2019**, *19*, 4211–4233.

51. Bergström, R.; Hallquist, M.; Simpson, D.; Wildt, J.; Mentel, T. F. Biotic stress: a significant contributor to organic aerosol in Europe?, *Atmos. Chem. Phys.* **2014**, *14*, 13643-13660.

52. Mareckova, K.; Wankmueller, R.; Anderl, M.; Poupa, S.; and Wieser, M. Inventory Review 2009. Emission Data reported under the LRTAP Convention and NEC Directive. Stage 1 and 2 review. Status of gridded data and LPS data. EMEP/CEIP Technical Report 1/2009, Umweltbundesamt GmbH, Vienna, Austria, 2009.

53. Wiedinmyer, C.; Akagi, S. K.; Yokelson, R. J.; Emmons, L. K.; Al-Saadi, J. A.; Orlando, J. J.; Soja, A. J. The Fire Inventory from NCAR (FINN): a high resolution global model to estimate the emissions from open burning, *Geosci. Model Dev.* **2011**, *4*, 625–641.

54. Janhäll, S.; Andersson, P. U.; Olofson, K. F. G.; Pettersson, J. B. C.; Hallquist, M. Evolution of the Urban Aerosol during Winter Temperature Inversion Episodes, *Atmos. Environ.* **2006**, *28*, 5355–5366.

55. Olofson, K. F. G. Andersson, P. U.; Hallquist, M.; Ljungström, E.; Tang, L.; Chen, D.; Pettersson, J. B. C. Urban aerosol evolution and particle formation during wintertime temperature inversions. *Atmos. Environ.*, **2008**, *43*, 340–346.

56. Roy, D. P.; Borak, J. S.; Devadiga, S.; Wolfe, R. E.; Zheng, M.; Descloitres, J. The MODIS Land product quality assessment approach, *Remote Sens. Environ.* **2002**, *83*, 62–76.

57. Ooki, A.; Uematsu, M.; Miura, K.; Nakae, S. Sources of sodium in atmospheric fine particles. *Atmos. Environ.* **2002,** *36*, 4367–4374.

58. Mamane, Y. Estimate of Municipal Refuse Incinerator Contribution to Philadelphia Aerosol .1. Source Analysis. *Atmos. Environ.* **1988**, *22*, 2411–2418.

59. Stohl, A.; Berg, T.; Burkhart, J. F.; Fjaeraa, A. M.; Forster, C.; Herber, A.; Hov, O.; Lunder, C.; McMillan, W. W.; Oltmans, S.; Shiobara, M.; Simpson, D.; Solberg, S.; Stebel, K.; Strom, J.; Torseth, K.; Treffeisen, R.; Virkkunen, K.; Yttri, K. E. Arctic smoke - record high air pollution levels in the European Arctic due to agricultural fires in Eastern Europe in spring 2006, *Atmos. Chem. Phys.* **2007**, *7*, 511-534.

60. Zhou, L.; Hopke, P.K.; Venkatachari, P. Cluster analysis of single particle mass spectra measured at Flushing, NY, *Analytica. Chimica. Acta*. **2006**, *555*, 47–56.